

# Coordination of multiple appendages in drag-based swimming

Silas Alben<sup>1,\*</sup>, Kevin Spears<sup>1</sup>, Stephen Garth<sup>1</sup>, David Murphy<sup>2</sup>  
and Jeannette Yen<sup>2</sup>

<sup>1</sup>*School of Mathematics, and* <sup>2</sup>*School of Biology, Georgia Institute of Technology, Atlanta, GA 30332-0160, USA*

Krill are aquatic crustaceans that engage in long distance migrations, either vertically in the water column or horizontally for 10 km (over 200 000 body lengths) per day. Hence efficient locomotory performance is crucial for their survival. We study the swimming kinematics of krill using a combination of experiment and analysis. We quantify the propulsor kinematics for tethered and freely swimming krill in experiments, and find kinematics that are very nearly metachronal. We then formulate a drag coefficient model which compares metachronal, synchronous and intermediate motions for a freely swimming body with two legs. With fixed leg velocity amplitude, metachronal kinematics give the highest average body speed for both linear and quadratic drag laws. The same result holds for five legs with the quadratic drag law. When metachronal kinematics is perturbed towards synchronous kinematics, an analysis shows that the velocity increase on the power stroke is outweighed by the velocity decrease on the recovery stroke. With fixed time-averaged work done by the legs, metachronal kinematics again gives the highest average body speed, although the advantage over synchronous kinematics is reduced.

**Keywords:** locomotion; krill; appendage; rowing; synchronous; metachronal

## 1. INTRODUCTION

Many locomotory behaviours in fluids can be classified as lift-based or drag-based (Childress 1981; Blake 1983; Vogel 1994). Lift-based locomotion involves a thin appendage flapping with a low angle of attack, which produces circulation by shedding vortices from its trailing edge. Circulation results in a lift force on the appendage, which has a component in the direction of the body's forward motion. At smaller scales, and for organisms which swim and crawl with the same appendages, drag-based swimming is common. Here the motion consists of alternating power and recovery strokes. In the power stroke the appendage is moved oppositely to the body's direction of motion with a large profile area, resulting in a large drag force propelling the body forward. On the recovery stroke the appendage is moved in the body's direction of motion with a small profile area, resulting in a small drag force opposite to the direction of motion.

Lift-based swimming is generally more efficient than drag-based swimming at high Reynolds numbers. Using a force coefficient model, Walker & Westneat (2000) found that drag-based swimming can be more effective at generating the large forces needed for manoeuvring. At low Reynolds numbers, lift-based swimming becomes ineffective (Alben & Shelley 2005; Alben 2008). Also, appendages suitable for lift-based

swimming are often not suitable for crawling behaviours. Thus, most aquatic arthropods (including crustaceans and insects) use drag-based swimming. These organisms typically move their appendages *metachronally*, meaning that the periodic motions of neighbouring appendages are shifted in time relative to one another (Morgan 1972). Metachronal motions are to be contrasted with synchronous motions, in which all appendages move together. The metachronal motion is used in both crawling and swimming, although the frequency and amplitude differ in the two cases. In this work, we consider the effectiveness of metachronal swimming in multi-appendage drag-based locomotion. We use a drag coefficient model to compare metachronal with synchronous and intermediate kinematics.

As examples, we consider the metachronal swimming motions of tethered and free krill. Krill are aquatic crustaceans (2–6 cm) that often engage in long distance migrations, either vertically over hundreds of metres in the water column (as part of the deep scattering layer) or horizontally for 10 km (over 200 000 body lengths) per day (Kils 1981). One species of krill, *Euphausia superba*, a key species that supports the high productivity of the Southern Oceans, consists of about 500 million tons of biomass or about five times the biomass of humans on earth (Nicol & Endo 1997). In contrast to fish, krill have articulated skeletons and rely on five pairs of appendages for multi-oared propulsion. The typical Reynolds number of the flow around

\*Author for correspondence (alben@math.gatech.edu).

the swimming krill body and appendages is  $10^2$ – $10^4$  (Yen *et al.* 2003; Swadlow *et al.* 2005), which is large enough for lift-based locomotion, although drag-based locomotion is used. Here, we build and test a model to evaluate how coordinated movements of the multiple appendages of this aquatic crustacean contribute to the efficiency of locomotion. For a high-biomass, highly migratory organism such as krill, efficient locomotory performance is crucial for survival. For some crustaceans (Alexander 1988) and most copepods (van Duren & Videler 2003), the power stroke is metachronal and the recovery stroke is synchronous. The organism changes its swimming speed by changing the frequency, and to some extent the amplitude, of the appendage motion (Kils 1981).

The sport of rowing provides another example of drag-based propulsion with multiple appendages (oars). Coordination is important, and, in nearly all instances of athletic rowing, all of the oars on the boat are synchronized (Wing & Woodburn 1995; Baudouin & Hawkins 2004). There has been some speculation but little systematic study of the possible advantages of asynchronous oar strokes. A brief article in *Rowing News* (Nolte 2007) mentioned tests of ‘syncopated’ rowing by the Soviet Union national rowing team in the 1980s, and asserted that a boat moving at constant speed would require 2.5 per cent less energy to cover the same distance as that covered with normal speed variations. Newspapers and films covered similar tests by the London Rowing Club in the 1920s (Neumeister 2004). In these cases, the oar strokes are staggered so that half the rowers perform a power stroke while the other half perform the recovery stroke. Human rowing has historical, psychological and geometrical aspects which could lead to a bias in favour of synchronous strokes. For rowers already trained to row synchronously, it may require many hours of training in the metachronal motion for rowers to outperform the synchronous motion. Also, slight deviations from synchronized strokes can induce yawing moments in the boat (Wing & Woodburn 1995), though the metachronal strokes we have mentioned avoid these yawing moments. Hence a synchronous rowing motion for a boat may be a local rather than a global optimum in the space of kinematics. Finally, there is evidence that synchrony can elevate pain thresholds of human rowers (Cohen *et al.* 2010). In this work, we use krill swimming as an example for a fairly general analysis of the differences between metachronal and synchronous rowing motions. A more specialized analysis may be required to understand the occurrence of metachronal or synchronous motions in particular organisms.

## 2. EXAMPLE OF METACHRONAL SWIMMING BY KRILL

### 2.1. Methods

Pacific krill (*Euphausia pacifica*) were collected off the coast of Oregon, USA, sorted into 2 l jars, and shipped overnight in an insulated container to Atlanta (courtesy of Bill Peterson, Hatfield Marine Center, Newport, OR).

Several of these shipments were made during the summers of 2008 and 2009. Upon arrival, the animals were placed either in 1 gallon glass jars with gentle aeration or in a 100 l recirculating kreisel tank (Hamner 1990). Both aquaria contained artificial seawater with a salinity of 35 ppt and were kept in a temperature-controlled cold room at 12°C. Krill that arrived in good condition exhibited normal swimming behaviour and lived for up to two months. Animals were fed a mixture of *Rhodomonas* and *Artemia nauplii*. Freely swimming animals were filmed both *in situ* in the kreisel tank (with the recirculating water turned off) and in a variety of smaller aquaria (volume of about 5 l). Up to 15 animals were placed in the filming aquaria at any one time in order to increase the chances of an animal crossing the camera field of view. The freely swimming krill were filmed under halogen lighting with an AOS X-PRI high-speed camera (AOS Technologies AG) at 250 frames per second. The camera was manually triggered when the animal swam into the field of view. In order to film tethered animals, the krill were restrained (Yen *et al.* 2003) in a manner similar to tethering copepods as described in Catton *et al.* (2007). The krill were tethered to a 38 gauge copper wire using cyanoacrylate glue. Attachments were made to the dorsal side of the krill near the junction between the cephalic and thoracic segments. A 0.5 mm bend at the end of the wire provided enough surface area for attachment. The end of the wire was dipped in glue and air-dried for 30 s until the glue was tacky, and then attached to a krill, which was restrained in a pool of water in a cooled Petri dish. Just prior to attachment, the krill was blotted dry of seawater for less than 1 s. Once the tacky end of the wire made contact with the dorsal side of the krill, ambient seawater was added to harden the glue and ensure attachment. The krill was fully submerged in artificial seawater (salinity of 35 ppt), and the krill–wire bond was checked for proper attachment and positioning. The wire was attached via a glass rod to a three-axis precision position manipulator, which was used to position the krill in the centre of the field of view of the camera. The tethered animals exhibited pleopod kinematics characteristic of locomotion and were filmed using the same camera and frame rate as for the freely swimming krill. Both lateral and ventral views of the tethered animal were filmed. Approximately 10 animals were filmed in the tethered state.

The pleopod kinematics of the Pacific krill, both freely swimming and tethered, were extracted from lateral view videos using the NIH IMAGEJ software. Of particular interest were the proximal segments of the pleopods (the protopodites). Two points on each pleopod, the protopodite base and tip, were manually digitized. For each pleopod pair, the angle between the long axis of the body and the protopodite was measured (see figure 1*b* for examples of angles). One arm of this angle was the ray between the protopodite base and tip. The other arm consisted of the ray between the protopodite base and the protopodite base of the next most anterior pleopod. In calculating this angle for the most anterior pleopod pair (pleopod pair 1), the ray from the second pleopod pair was used.

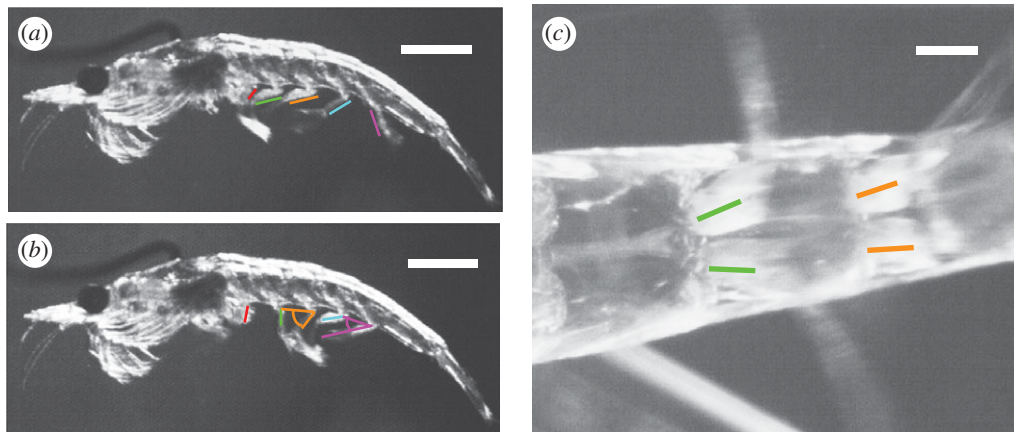


Figure 1. Kinematics of thrust-producing appendages of krill. (a,b) Side views of a tethered krill at two different instants of its periodic swimming motion. The proximal segments (protopodites) of the five pleopods are highlighted with coloured lines (from front to rear: red, green, orange, cyan, purple). In (a) the rays parallel to the protopodites are displaced from the protopodites so as not to obscure them. In (b), the angle between the protopodite and the body axis is shown for the third and fifth pleopod pair. (c) A bottom view of the second and third pleopod pairs (green and orange) during the power stroke of the second pleopod pair and the beginning of the recovery stroke of the third. Scale bars: (a,b), 5 mm; (c), 1 mm.

## 2.2. Krill pleopod kinematics

In figure 1a,b we show two side views of the krill during tethered swimming, at different instants during the stroke cycle. Coloured line segments are drawn next to the first joint of each of the five pleopods. In figure 1c, a bottom view is shown at an instant during the power stroke of the second pleopod (green, as in figure 1a,b) and the beginning of the recovery stroke of the third pleopod (orange, as in figure 1a,b). This view shows that each pleopod is a paired structure, symmetric about the body midline. The white streaks extending outward to each side of the body from the ends of the second pleopod are thin panel structures called ‘exopodites’. These structures move outward from the body during the power stroke, and inward during the recovery stroke. They therefore increase the profile area during the power stroke, which increases the net thrust force on the pleopod. For the third pleopod (orange) in figure 1c, the exopodites are almost fully retracted towards the body, because this pleopod is beginning the recovery stroke.

In figure 2a, we plot the angles of the proximal segments of the five pleopod pairs during four consecutive stroke periods of tethered swimming. The data for each of the pleopods are plotted in a different colour, which correspond to the colour labelling in figure 1. The angle plotted is that shown in figure 1b: the angle between the proximal pleopod segment and the tangent to the krill body, in the forward direction, where it meets the pleopod. The motion is very close to periodic in time. We plot the average of the data over the four cycles in figure 2b. The last pleopod moves with the largest amplitude, and the phase between successive pleopods is fairly uniform, showing a good approximation to metachronal kinematics. In figure 2c, we plot a schematic of the pleopod motions during a cycle, using the angle data from figure 2b. The fifth pleopod (purple) leads both the power and recovery strokes, and the wave of motion propagates forward along the krill body. In figure 2d–f, we plot

the same quantities but now for *freely* swimming krill. The data, shown in figure 2d, extend over a somewhat shorter time range, about 2.5 stroke periods. The average of the stroke data over the two stroke periods starting with the recovery stroke of the fifth pleopod (purple) is shown in figure 2e. There are two main differences from the tethered data. First, the stroke period for free swimming is about 4 per cent shorter: 0.092 s versus 0.096 s. Second, the free-swimming data are closer to metachronal, which can be seen by comparing figure 2e with figure 2b. In figure 2b the phase difference between the first and fifth pleopods is shorter than that between the others, while in figure 2e the phase differences between adjacent pleopods in the stroke cycle are more nearly uniform. In both the tethered and free cases, the fifth pleopod has the largest amplitude and the wave of motion passes from the fifth pleopod to the first.

We may estimate a Reynolds number for the pleopod motion using a typical length  $L$  of a pleopod (0.5 cm), an average velocity  $U$  at the distal tip ( $20 \text{ cm s}^{-1}$ ) and the kinematic viscosity  $\nu$  of seawater at  $12^\circ\text{C}$  ( $0.013 \text{ cm}^2 \text{ s}^{-1}$ ; Billings *et al.* 1963):  $Re = UL/\nu = 770$ .

## 3. DRAG COEFFICIENT MODEL

We consider drag-based swimming involving high Reynolds number flow past a bluff body. It is difficult to capture the detailed hydrodynamics of such wake flows in a simple model. We thus propose a model for multi-appendage drag-based swimming where the fluid dynamics is represented using drag coefficients. Similar drag coefficients have been used in previous studies of rowing (Blake 1981; Walker & Westneat 2000; Cabrera *et al.* 2006). Our model neglects the fluid dynamical interactions between the appendages and the body, which are fully three-dimensional for krill. Such interactions are likely to be significant when the pleopods are nearly in contact with each other and the krill body. However, our drag coefficient

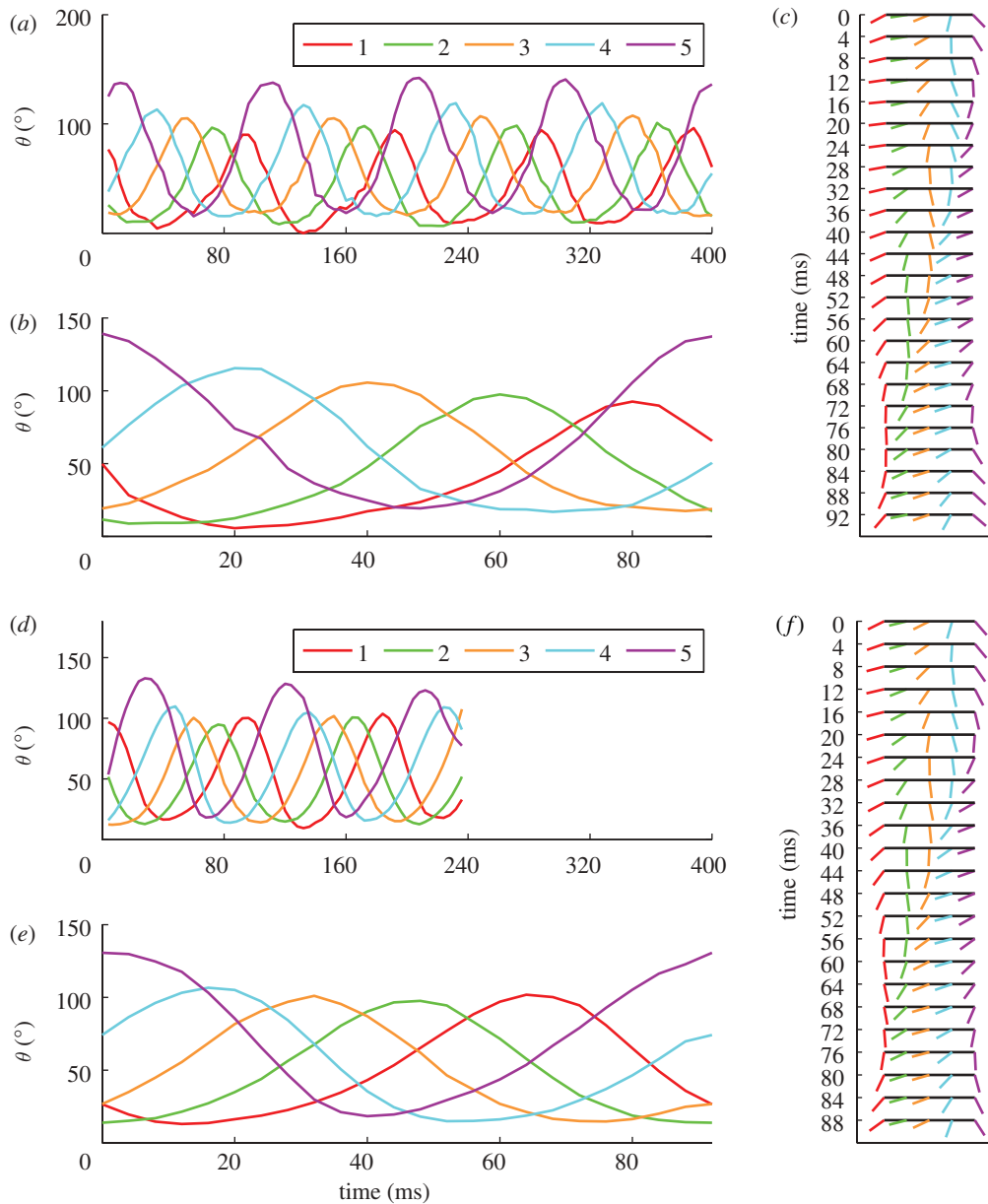


Figure 2. The orientations of the proximal segments of the five pleopods (1, red; 2, green; 3, orange; 4, cyan; and 5, purple) versus time during the tethered swimming motion. (a) The five pleopods are labelled with the same colours as in figure 1*a,b*, and are tracked over four periods. (b) The average orientations over a period. At each time, we plot the average of the four values at the same times, relative to the period duration, from the four periods of data in (a). (c) A schematic showing the orientations of the pleopods (coloured lines) relative to the body (black line) over a period, from the data in (b). (d–f) The same quantities as in (a–c) but for freely swimming krill, with the following modification. The data shown in (d) run over only 2.5 stroke cycles. Two of the stroke cycles are averaged to give the data in (e).

model is much simpler to analyse than a three-dimensional flow simulation, and thus allows a much wider investigation of parameter space. We use the model to consider how the relative timing of the appendages affects swimming performance. For the model, we call each pleopod pair a ‘leg’, to use a more common term. We first consider a body with two legs instead of five pleopod pairs (as for the krill), and address the case of more than two legs subsequently. Our model determines the body velocity  $v(t)$  for a class of simple periodic swimming motions.

We use a local approximation for the fluid force on each leg and the body, similar to those used in ordinary differential equation models of rising bubbles and

falling paper (Rensen *et al.* 2001; Andersen *et al.* 2005). The force on each leg and on the body is proportional to their velocities relative to the fluid, raised to the power 1 or 2. The constant of proportionality is a drag coefficient, which depends on the shape and profile area of the leg or body (Batchelor 1967). The drag coefficient for each leg in the power stroke is  $c_p$ , and in the recovery stroke is  $c_r$ . The drag coefficient for the body is  $c_b$ . We assume  $c_b > c_p > c_r > 0$ , since the body is usually much larger than the appendages. We relate these drag coefficients to the more common drag coefficient  $C_D$  in appendix A.

We define time  $t = 0$  to be the instant when leg 1 switches from a recovery stroke (with constant velocity

–1) to a power stroke (with constant velocity 1). At time  $t = t_1 > 0$ , leg 2 switches from a recovery stroke to a power stroke. At time 0.5, leg 1 switches back to a recovery stroke, and at time  $0.5 + t_1$ , leg 2 switches back to a recovery stroke. Over one period of motion, the leg kinematics thus switch four times, yielding a sequence of four ordinary differential equations to be satisfied in a period of motion,

$$\begin{aligned} \dot{v} = & -c_b \operatorname{sgn}(v)|v|^\alpha + c_p \operatorname{sgn}(1-v)|1-v|^\alpha \\ & -c_r \operatorname{sgn}(1+v)|1+v|^\alpha, \quad 0 < t < t_1, \end{aligned} \quad (3.1)$$

$$\begin{aligned} \dot{v} = & -c_b \operatorname{sgn}(v)|v|^\alpha + 2c_p \operatorname{sgn}(1-v)|1-v|^\alpha, \\ & t_1 < t < 0.5, \end{aligned} \quad (3.2)$$

$$\begin{aligned} \dot{v} = & -c_b \operatorname{sgn}(v)|v|^\alpha + c_p \operatorname{sgn}(1-v)|1-v|^\alpha \\ & -c_r \operatorname{sgn}(1+v)|1+v|^\alpha, \\ & 0.5 < t < 0.5 + t_1 \end{aligned} \quad (3.3)$$

and

$$\begin{aligned} \dot{v} = & -c_b \operatorname{sgn}(v)|v|^\alpha - 2c_r \operatorname{sgn}(1+v)|1+v|^\alpha, \\ & 0.5 + t_1 < t < 1. \end{aligned} \quad (3.4)$$

We solve the equations with the boundary conditions that the velocity is continuous at  $t = t_1, 0.5, 0.5 + t_1$  and  $v(0) = v(1)$ . Since the forces (and thus accelerations) are finite, the velocity is continuous throughout the motion. Here  $\operatorname{sgn}$  is the signum function and  $v$  is the body velocity. The variables are dimensionless: time is non-dimensionalized by the stroke period, velocity is non-dimensionalized by the leg speed, and mass is non-dimensionalized by the body mass. Equations (3.1)–(3.4) show that the body velocity is continuously changing in response to a changing balance of forces. The body drag term (proportional to  $c_b$ ) tends to decrease the body speed. The leg power and recovery terms (proportional to  $c_p$  and  $c_r$ , respectively) tend to move the body velocity towards the values  $+1$  and  $-1$ , respectively, which are minus the velocity of the legs. Hence the body velocity is confined to the range  $-1 < v < 1$  during the cycle. Since  $c_p > c_r$ , the average body velocity over a period lies between 0 and 1.

Here drag is proportional to velocity raised to a power  $\alpha$  which may be 1 or 2. When  $\alpha = 2$ , drag is proportional to velocity squared, appropriate for high Reynolds number flows typical for swimming krill, fish, birds and mammals (Vogel 1994). A combination of terms with  $\alpha = 1$  and 2 or intermediate values has been used to model drag at intermediate Reynolds numbers (Brown & Lawler 2003; Thompson & Smith 2004). For generality, we consider both  $\alpha = 1$  and 2 in this work, with the expectation that intermediate cases will be interpolated to some extent by the extreme cases. A linear drag law is appropriate for Reynolds numbers below 1, which includes swimming by microorganisms (Childress 1981). Metachronal swimming motions of cilia and flagella are typical at low Reynolds number.

Some previous work has attributed the advantages of metachronal swimming to the fact that synchronous swimming leads to higher fluctuations in body velocity

(Hill & Fahrig 2009). If the drag law is quadratic in velocity, it is plausible that the increase in body drag during the power stroke outweighs the decrease in body drag during the recovery stroke, leading to a smaller average body velocity. This intuition does not address the legs, however, which may gain from velocity fluctuations because they move in opposition to the body. It is also unclear whether the intuition applies when drag is linear in velocity. A goal of the model is to test this intuition in a generic situation.

In all cases our model is simple enough to be solved with elementary methods, in terms of exponential functions. For  $\alpha = 1$ , the body velocity is a constant plus an exponential function on each of the four subintervals in time. For  $\alpha = 2$ , the body velocity is a ratio of such functions on each subinterval. Imposing the boundary conditions (that body velocity is continuous in time) fixes constants in these solutions.

Although our model is simple, it still contains five parameters:  $c_b, c_p, c_r, \alpha$  and  $t_1$ . We can simplify the problem by focusing on the most important range of parameter space. We consider just two values of  $\alpha$ : 1 and 2.  $\alpha = 2$  is the appropriate value for krill, but for comparison we also consider  $\alpha = 1$ , important at lower Reynolds numbers. A second simplifying fact is that the legs are much smaller than the body. The drag coefficients  $c_b, c_p$  and  $c_r$  scale with the profile area (see appendix A), and by using images such as figure 1 we may estimate the length and width of the pleopods on the power and recovery strokes. We estimate the typical magnitudes of  $c_b, c_p$  and  $c_r$  in appendix A, and obtain  $c_b = 0.3, c_p = 0.06$  and  $c_r = 0.03$ . We also consider larger values of  $c_b, c_p$  and  $c_r$  to understand how the body mass plus added mass affects the results. One expects larger body mass plus added mass to result in a slower approach to the equilibrium swimming speed on each subinterval, and this is borne out by the results we now present. The power coefficient  $c_p$  is estimated using the profile area of a pleopod on the power stroke. The increase in profile area of the pleopods is due to the rapid expansion of the exopodites on the power stroke, which is difficult to measure precisely. We thus allow  $c_p/c_r$  to vary in the range 1.2–7.

We first consider solutions for  $\alpha = 1$ . Some typical solutions are shown in figure 3. In figure 3a, the legs move synchronously. Both legs execute the power stroke for  $0 < t < 0.5$ , and the body velocity increases as a saturating exponential curve. Both legs execute the recovery stroke for  $0.5 < t < 1$ , and the body velocity decreases as a (different) saturating exponential curve. In figure 3b, the drag coefficients for the body and for the legs are the same as in figure 3a, but the legs now move with different phases. Since each leg has two switching times in a period (from power stroke to recovery stroke and from recovery stroke back to power stroke), there are now four subintervals in alternating grey and black (corresponding to the sequence of four equations (3.1)–(3.4)). In each of the four subintervals, there is a unique equilibrium solution to the corresponding equations (3.1)–(3.4), given by the values of  $v$  at which the right-hand sides of equations (3.1)–(3.4) are zero, and thus  $\dot{v} = 0$ . The equilibria

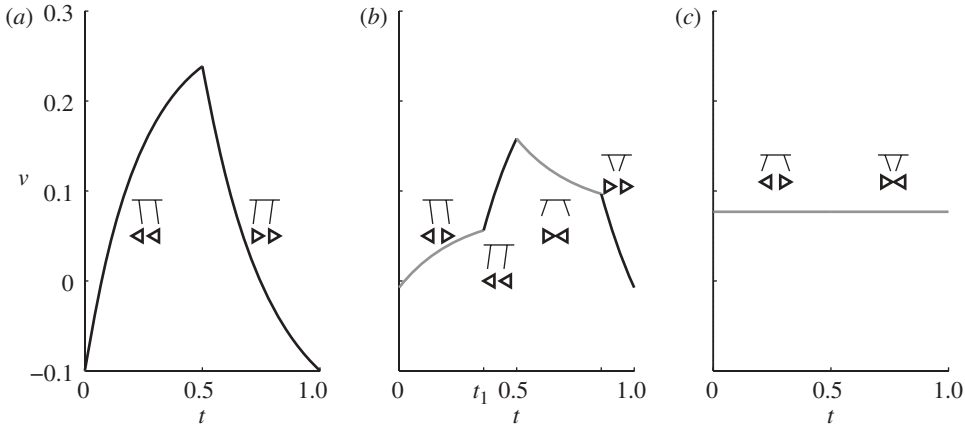


Figure 3. Three examples of model krill body velocity dynamics for different leg phases: (a) synchronous, (b) intermediate and (c) metachronal. Plotted is the body speed in the linear drag coefficient model over one period of time. The body speed is the solution to equations (3.1)–(3.4) with the phase shifts (a)  $t_1 = 0$  (synchronous), (b)  $t_1 = 0.36$  (intermediate) and (c)  $t_1 = 0.5$  (metachronal). Here the body drag coefficient is  $c_b = 3$ , power drag coefficient is  $c_p = 0.6$  and recovery drag coefficient is  $c_r = 0.3$ . In each of the four phases, a schematic of the model body and legs is shown, with the arrows indicating leg motion to the left during the power stroke and to the right during the recovery stroke.

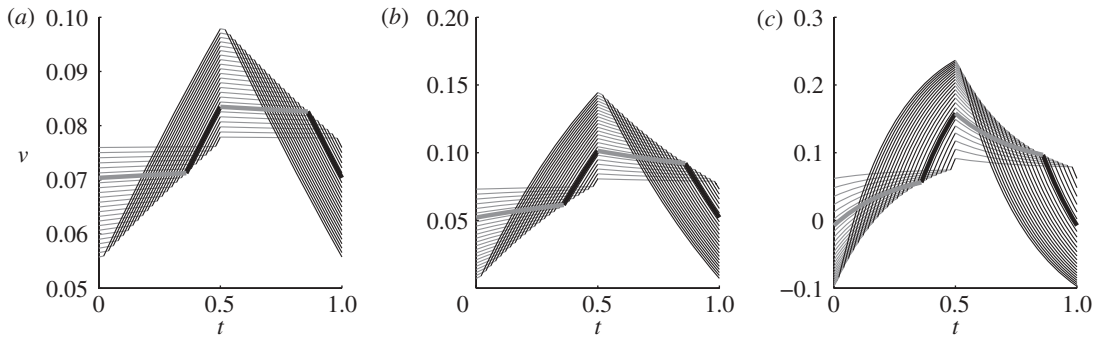


Figure 4. For the linear drag law model, the body velocity over a period for the phase shift between the legs  $t_1$  varying from 0.48 down to 0.02. In each panel the ratio of body drag coefficient to power drag coefficient to recovery drag coefficient ( $c_b : c_p : c_r$ ) is the same (1 : 0.2 : 0.1) but is multiplied by a constant factor of (a) 0.3, (b) 1 and (c) 3. In each panel the single trajectory with phase  $t_1 = 0.36$  is given with thick lines, as an example.

are attracting, and the body velocity tends to the equilibria as a saturating exponential curve. At the transitions between the four subintervals, the value of the equilibrium changes discontinuously. The body velocity at the end of a given subinterval is the initial condition for the next subinterval, where there is an exponential approach to a different equilibrium. This example uses  $t_1 = 0.36$ , which is an intermediate case between synchronous ( $t_1 = 0$ ) and metachronal ( $t_1 = 0.5$ ) kinematics. Figure 3c shows the body velocity for metachronal kinematics. Now the velocity is constant in time, because at every instant there is one leg on the power stroke and one on the recovery stroke, so the body is always at the equilibrium solutions to equations (3.1) and (3.3) (which are equal). The largest fluctuations in body velocity occur for synchronous leg motions, and the smallest (no fluctuation) occurs for metachronal leg motions, as expected.

In figure 4, we show the curves for various phases  $t_1$  ranging from zero (synchronous, i.e. legs with the same phase) to one-half (metachronal, i.e. legs with opposite phase), and various drag coefficients. Figure 4c shows the full range of intermediate cases between the

synchronous case in figure 3a and the metachronal case in figure 3c. The highlighted trajectory in figure 4c is the trajectory shown in figure 3b. The body velocity approaches the flat line of figure 3c when  $t_1$  approaches 0.5, corresponding to metachronal kinematics. While there is more fluctuation in body velocity with a more synchronous stroke, it is not obvious whether the *time-averaged* velocity varies much. This question is addressed by the results in figure 5. We plot the mean velocity versus phase, for many combinations of  $c_p$  and  $c_r$ . Each of the trajectories in figure 4a–c has an average velocity that corresponds to one of the crosses in figure 5b. There are three curves in figure 5b. The curve with the largest fluctuation (minimum velocity 0.073) corresponds to the trajectories in figure 4c. The curve in the middle corresponds to the trajectories in figure 4b, and the highest, nearly flat curve corresponds to figure 4a. For all three curves in figure 5b, metachronal motion ( $t_1 = 0.5$ ) gives the highest average velocity. Figure 5a plots results for the same situation as in figure 5b but with a larger power drag coefficient  $c_p$ . Consequently, the body velocity is larger in figure 5a. In figure 5c, the power

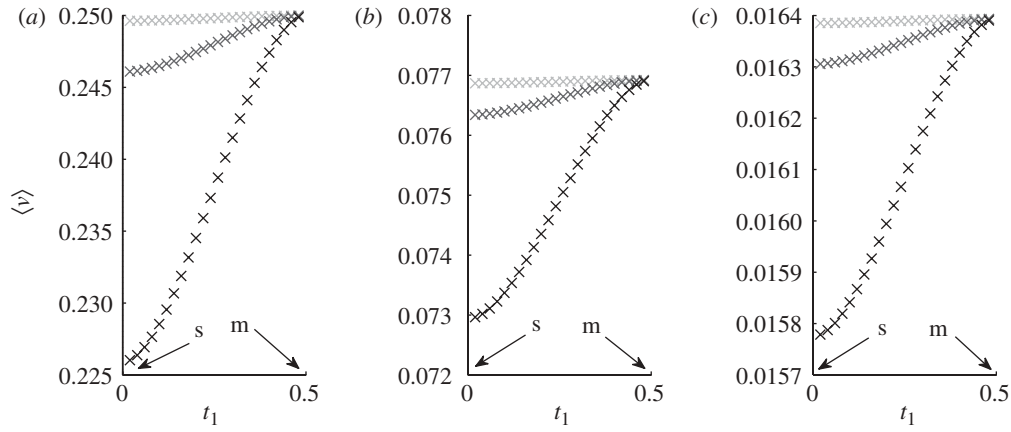


Figure 5. For the linear drag law model, the average body velocity versus the phase difference between the legs,  $t_1$ . Each panel uses a different value of  $c_p$ , the drag coefficient on the power stroke. The relative magnitudes of the drag coefficients are:  $c_b : c_p : c_r = 1 : 0.5 : 0.1$  (a),  $1 : 0.2 : 0.1$  (b) and  $1 : 0.12 : 0.1$  (c). Within each panel, the three curves of crosses are data for three multiples of the given ratio of drag coefficients: 0.3 (light grey), 1 (dark grey), and 3 (black). Higher magnitudes of the drag coefficients correspond to a larger difference between the body velocity at the synchronous phase (indicated by arrow labelled ‘s’) and the metachronal phase (indicated by arrow labelled ‘m’). The data in (b) correspond to the plots in figure 4.

coefficient is reduced and so is the body velocity. The important fact is that the curves have nearly the same shape in figure 5a–c, even though the velocity magnitudes and the differences between power and recovery drag coefficients vary greatly. The metachronal motion achieves the highest velocity in all cases, and the synchronous motion gives the lowest velocity.

For the linear drag law ( $\alpha = 1$ ), it is possible to obtain simple expressions for the average body velocity during synchronous ( $t_1 = 0$ ) and metachronal ( $t_1 = 0.5$ ) kinematics, and to compare the two directly. For metachronal kinematics, equations (3.1)–(3.4) reduce to the single equation (3.1) during the entire period. Owing to the periodic boundary conditions, the velocity is a constant given by

$$v_m = \frac{c_p - c_r}{c_b + c_p + c_r}. \quad (3.5)$$

For synchronous kinematics, the four phases given by equations (3.1)–(3.4) reduce to the two phases given by equations (3.2) and (3.4). The average swimming velocity for synchronous kinematics can be written as

$$v_s = \int_0^1 v dt = v_{\text{eq}}^{\text{avg}} + (v_m - v_{\text{eq}}^{\text{avg}})f(c_{pb}, c_{rb}), \quad (3.6)$$

$$f(c_{pb}, c_{rb}) = \frac{\sinh(c_{pb}) \sinh(c_{rb})}{c_{pb} c_{rb}} \frac{c_{pb} + c_{rb}}{\sinh(c_{pb} + c_{rb})}, \quad (3.7)$$

$$c_{pb} = \frac{c_b + 2c_p}{4}, \quad c_{rb} = \frac{c_b + 2c_r}{4}$$

and

$$v_{\text{eq}}^{\text{avg}} = \frac{1}{2} \left( \frac{2c_p}{c_b + 2c_p} + \frac{-2c_r}{c_b + 2c_r} \right). \quad (3.8)$$

Here  $v_{\text{eq}}^{\text{avg}}$  is the average of the equilibrium swimming velocities in the two phases (power and recovery). The function  $f(c_{pb}, c_{rb})$ , plotted in figure 6, is bounded between 0 and 1. Hence  $v_s$  in equation (3.6) ranges between  $v_m$ , the metachronal velocity, and  $v_{\text{eq}}^{\text{avg}}$ . The

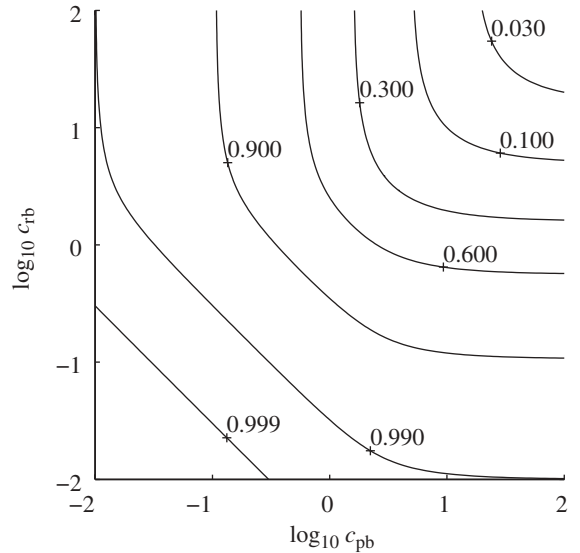


Figure 6. The factor  $f$  in equation (3.7) for different values of the modified power and recovery coefficients  $c_{pb}$  and  $c_{rb}$ , showing the transition in body speed for synchronous leg kinematics, from  $v_m$  (where  $f = 1$ ) to  $v_s$  (where  $f = 0$ ).

ratio of the synchronous velocity to the metachronal velocity is

$$\frac{v_s}{v_m} = (1 - f(c_{pb}, c_{rb})) \frac{c_b}{c_b + 2c_r} \frac{c_b + c_p + c_r}{c_b + 2c_p} + f(c_{pb}, c_{rb}), \quad (3.9)$$

which ranges between  $\frac{1}{3}$  and 1 for  $c_b > c_p > c_r > 0$ .

When  $c_b, c_p, c_r \rightarrow 0$ , the inertia of the body is large, so the velocity is nearly constant. Setting  $\dot{v}$  to zero and equating  $v$  in equations (3.2) and (3.4), we obtain  $v_s = v_m$ . Intuitively, the large inertia of the body causes the power and recovery forces on the body to be averaged in time, so the result is the same as if the forces were applied simultaneously, which gives metachronal kinematics. When  $c_b, c_p, c_r \rightarrow \infty$ , the inertia of the body is small, so in each of the phases given by equations

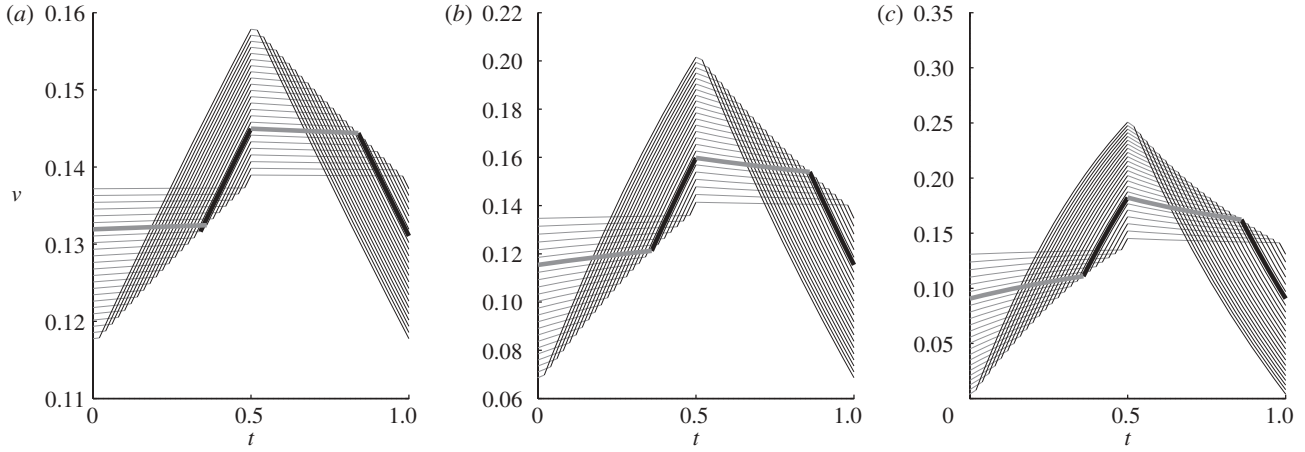


Figure 7. For the quadratic drag law model, the body velocity over a period for the phase shift between the legs  $t_1$  varying from 0.48 down to 0.02. In each panel the ratio  $c_b : c_p : c_r$  is the same (1 : 0.2 : 0.1) but is multiplied by a constant factor of (a) 0.3, (b) 1 and (c) 1.9. In each panel the single trajectory with phase  $t_1 = 0.36$  is given with thick lines, as an example. The attracting equilibrium on subintervals 1 and 3 is 0.138; on subinterval 2 it is 0.387. There are complex-conjugate equilibria on subinterval 4:  $(-0.167 \pm 0.372i)$ .

(3.2) and (3.4) the body rapidly moves to its equilibrium speed for that phase. Hence  $v_s = v_{\text{eq}}^{\text{avg}}$  in this case.

We have found analytically that metachronal kinematics give a faster average body speed than synchronous kinematics for the linear drag law. We now give a second analysis that shows that metachronal kinematics is a local optimum, for both the linear and quadratic drag laws. In other words, a slight change in phase from metachronal towards more synchronous kinematics leads to a decrease in the average body speed.

We thus consider the case where the phase is perturbed by  $\varepsilon$  from metachronal kinematics, i.e.  $0 < 0.5 - t_1 = \varepsilon \ll 1$ . We expand the velocity as  $v = v_m + \tilde{v}$ , which is the metachronal velocity (for  $t_1 = 0.5$ ) plus a small perturbation  $\tilde{v}$ .

Using equations (3.1)–(3.4) in the linear case, we have

$$\dot{\tilde{v}} = (-c_b - c_p - c_r)\tilde{v}, \quad 0 < t < 0.5 - \varepsilon, \quad (3.10)$$

$$\dot{\tilde{v}} = (-c_b - 2c_p)\tilde{v} - c_b v_m + 2c_p(1 - v_m), \quad 0.5 - \varepsilon < t < 0.5, \quad (3.11)$$

$$\dot{\tilde{v}} = (-c_b - c_p - c_r)\tilde{v}, \quad 0.5 < t < 1 - \varepsilon \quad (3.12)$$

and

$$\dot{\tilde{v}} = (-c_b - 2c_r)\tilde{v} - c_b v_m - 2c_r(1 + v_m), \quad 1 - \varepsilon < t < 1. \quad (3.13)$$

During the combined power stroke ( $0.5 - \varepsilon < t < 0.5$ ), the change in body velocity can be expanded in powers of  $\varepsilon$  using the method of successive approximations on equation (3.11),

$$\Delta \tilde{v}_p = (-c_b v_m + 2c_p(1 - v_m))\varepsilon + (-c_b - 2c_p) \times (-c_b v_m + 2c_p(1 - v_m)) \frac{\varepsilon^2}{2} + O(\varepsilon^3). \quad (3.14)$$

During the combined recovery stroke, using equation (3.13), the change in body velocity is

$$\Delta \tilde{v}_r = (-c_b v_m - 2c_r(1 + v_m))\varepsilon + (-c_b - 2c_r) \times (-c_b v_m - 2c_r(1 + v_m)) \frac{\varepsilon^2}{2} + O(\varepsilon^3). \quad (3.15)$$

The  $O(\varepsilon)$  terms in equations (3.14) and (3.15) are equal in magnitude and opposite in sign, so they produce no net change from the metachronal velocity. However, the  $O(\varepsilon^2)$  term in  $\Delta \tilde{v}_p$  is negative and larger in magnitude than the positive  $O(\varepsilon^2)$  term in  $\Delta \tilde{v}_r$ . Hence the body velocity does not increase as much on the combined power stroke as it decreases on the combined recovery stroke. Thus, a slight move away from metachronal kinematics always decreases the average body velocity for the linear drag law.

For the quadratic drag law, the analogous velocity increments are

$$\Delta \tilde{v}_p = (-c_b v_m^2 + 2c_p(1 - v_m)^2)\varepsilon + (-2c_b v_m - 4c_p(1 - v_m)) \times (-c_b v_m^2 + 2c_p(1 - v_m)^2) \frac{\varepsilon^2}{2} + O(\varepsilon^3) \quad (3.16)$$

and

$$\Delta \tilde{v}_r = (-c_b v_m^2 - 2c_r(1 + v_m)^2)\varepsilon + (-2c_b v_m - 4c_r(1 + v_m)) \times (-c_b v_m^2 - 2c_r(1 + v_m)^2) \frac{\varepsilon^2}{2} + O(\varepsilon^3). \quad (3.17)$$

The  $O(\varepsilon)$  terms cancel here as well, and again, at  $O(\varepsilon^2)$ ,  $\Delta \tilde{v}_p$  gives a larger decrease than the increase from  $\Delta \tilde{v}_r$ . Again the body velocity decreases more on the combined recovery stroke than it increases on the combined power stroke.

In figure 7, we present solutions analogous to those of figure 4, but now with the quadratic drag law ( $\alpha = 2$ ). Now the right-hand sides of equations (3.1)–(3.4) are quadratic polynomials, with two roots which are the equilibrium values of the body velocity  $v$  on each

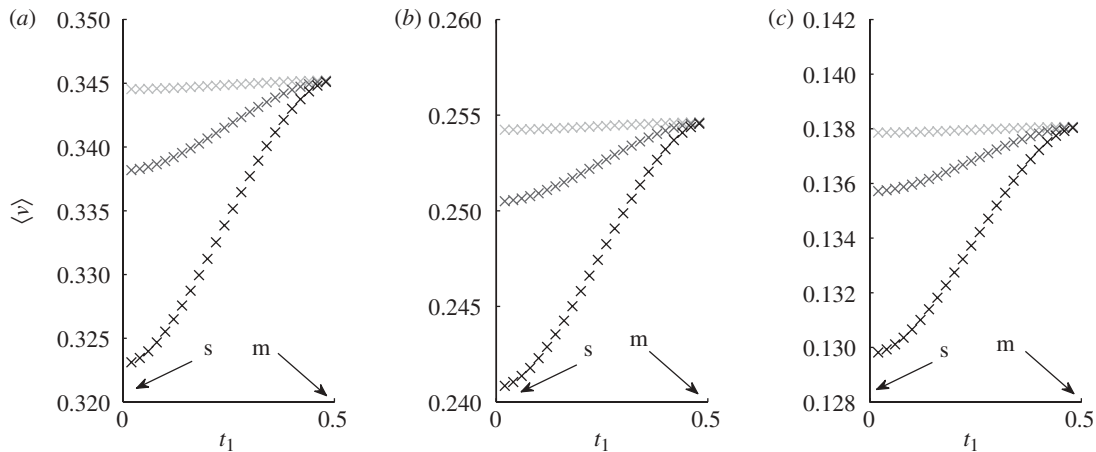


Figure 8. For the quadratic drag law model, the average body velocity versus the phase difference between the legs,  $t_1$ , for three values of the ratio  $c_b : c_p : c_r$ ,  $1 : 0.7 : 0.1$  (a),  $1 : 0.4 : 0.1$  (b) and  $1 : 0.2 : 0.1$  (c). In each panel, data are shown for three multiples of the given ratio: 0.3 (light grey), 1 (dark grey) and 1.9 (black). In each case curves with larger variations correspond to larger multiples. The data in (c) correspond to the plots in figure 7. The arrows labelled ‘s’ and ‘m’ show the values of  $t_1$  that correspond to synchronous and metachronal kinematics, respectively.

subinterval. In the four phases, the body velocity now evolves as a *ratio* of exponential functions of time.

In figure 8, we plot the average body velocities versus phase with the quadratic drag law, for various parameters, analogously to figure 5. In all cases, metachronal kinematics are optimal, and the velocity behaves quadratically near the optimum ( $t_1 = 0.5$ ), in accordance with equations (3.16) and (3.17).

### 3.1. Efficiency

We have shown that the body velocity is largest with metachronal kinematics, for fixed leg speed. Another important question is how the mechanical efficiency depends on the phase difference between the legs. Swimming is considered to be the dominant component of energy expenditure by krill (Swadling *et al.* 2005). Instead of using the same leg velocity for all phase differences, we now fix the average amount of work done on the fluid by the legs for all phase differences, and allow the leg velocity amplitude to vary to satisfy this constraint. We then ask: which phase difference between the legs yields the highest body velocity for fixed work?

We thus use equations (3.1)–(3.4) again, but change the terms  $1 \pm v$  to  $A \pm v$ . The leg velocity amplitude  $A$  is set by the constraint that the work  $W$  done by the legs on the fluid is constant as  $t_1$  is varied. The work is the time integral of the power, which is the force of the legs on the fluid multiplied by the legs’ velocities relative to the body

$$\begin{aligned}
 W = & A \int_0^{t_1} c_p \operatorname{sgn}(A - v) |A - v|^\alpha + c_r \operatorname{sgn}(A + v) |A + v|^\alpha dt \\
 & + A \int_{t_1}^{0.5} 2c_p \operatorname{sgn}(A - v) |A - v|^\alpha dt \\
 & + A \int_{0.5}^{t_1+0.5} c_p \operatorname{sgn}(A - v) |A - v|^\alpha \\
 & \quad + c_r \operatorname{sgn}(A + v) |A + v|^\alpha dt \\
 & + A \int_{t_1+0.5}^1 2c_r \operatorname{sgn}(A + v) |A + v|^\alpha dt. \quad (3.18)
 \end{aligned}$$

In figure 9, we plot the average body velocity  $\langle v \rangle$  and the leg velocity amplitude  $A$ , versus phase difference  $t_1$  for the linear drag case. We use the same force coefficients as in figure 5. Here the value of  $W$  is fixed for each curve, and is that which occurs for the metachronal cases ( $t_1 = 0.5$ ) in figure 5, for ease of comparison. Hence the velocity amplitudes for the metachronal cases only are the same (unity) in figures 5 and 9. We find that the metachronal kinematics are the most efficient (i.e. yield the highest swimming speed for a given input work) in all cases. However, the constraint of fixed work gives a higher leg speed for synchronous kinematics. Comparing with figure 5, we see that the speed advantage of metachronal over synchronous kinematics is reduced by approximately one-half when the input work is taken into account.

Figure 10 gives fixed-work results for the quadratic drag case, to be compared with figure 8. Again, the metachronal velocity advantage is reduced when the work is held fixed, though here the velocity reduction is smaller (20–30%) than in the linear case, where it was approximately 50 per cent.

### 3.2. More than two legs

In the case of  $n > 2$  legs undergoing metachronal kinematics, the model is nearly the same as the two-leg model. If the number of legs is even, there are equal numbers of legs in the power stroke and in the recovery stroke at a given time. The model then reduces to that with two legs, with the power and recovery coefficients multiplied by half the number of legs. For an odd number of legs, there is one additional leg in the power or recovery stroke at each time. Its relative effect is small when  $n$  is large. We consider the case where  $n = 5$  (which is not large) below.

For  $n$  legs undergoing synchronous kinematics, the model reduces to that with two legs, with the power and recovery coefficients multiplied by the number of legs. Thus, the two-leg model is representative of the many-leg model for synchronous and metachronal kinematics. For intermediate phase differences, both the

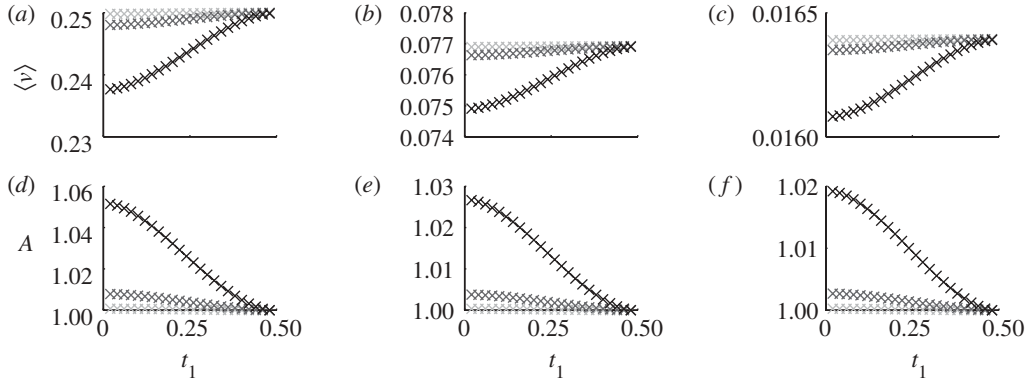


Figure 9. For the linear drag law model, the average body velocity  $\langle v \rangle$  (*a–c*) and leg velocity amplitude  $A$  (*d–f*) versus the phase difference between the legs,  $t_1$ , for fixed input work (equation (3.18)). The same values of the ratio  $c_b : c_p : c_r$  as in figure 5 are used: 1 : 0.5 : 0.1 (*a,d*), 1 : 0.2 : 0.1 (*b,e*), 1 : 0.12 : 0.1 (*c,f*). In each panel, data are shown for three multiples of the given ratio: 0.3 (light grey), 1 (dark grey) and 3 (black). In each case curves with larger variations correspond to larger multiples.

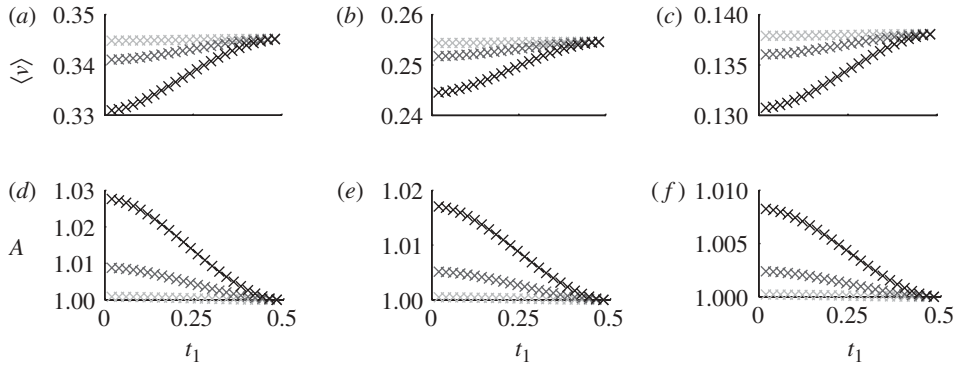


Figure 10. For the quadratic drag law model, the average body velocity  $\langle v \rangle$  (*a–c*) and leg velocity amplitude  $A$  (*d–f*) versus the phase difference between the legs,  $t_1$ , for fixed input work (equation (3.18)). The same values of the ratio  $c_b : c_p : c_r$  as in figure 8 are used: 1 : 0.7 : 0.1 (*a,d*), 1 : 0.4 : 0.1 (*b,e*), 1 : 0.2 : 0.1 (*c,f*). In each panel, data are shown for three multiples of the given ratio: 0.3 (light grey), 1 (dark grey) and 1.9 (black). In each case curves with larger variations correspond to larger multiples.

two-leg and many-leg models interpolate metachronal and synchronous kinematics, so the results in the two cases are expected to be qualitatively similar.

For the case of krill,  $n = 5$  and  $\alpha = 2$ . The relative phases of the five legs are described by four parameters (one leg may be chosen to begin its power stroke at  $t = 0$ ). We consider a one-dimensional slice through this four-dimensional parameter space, which includes both synchronous and metachronal kinematics. We assume that the five legs begin their power strokes at times separated by equal amounts  $t_1$ . When  $t_1 = 0$  (or 1) we have synchronous kinematics. When  $t_1 = 0.2, 0.4, 0.6$  or  $0.8$ , we have metachronal kinematics, which approximate well the kinematics we have given in §2.2.

In figure 11*a–c* we show time traces of body velocity for the five-leg case, analogously to figure 7, and with the same overall drag coefficients. With two legs, there were four phases of motion in a period for the general case (shown in figure 3*b*). Now, with five legs, there are 10 phases of motion, shown in alternating red and black in figure 11. There is a great deal of overlap among the 50 trajectories shown in figure 11*a–c*, but we can classify them into two groups. One group consists of trajectories that form a lattice-like pattern,

extending up to the highest velocity and down to the lowest velocity (0.16 and 0.12 in figure 11*a*, for example). These are the trajectories that are more synchronous, with  $t_1 < 0.15$  and  $t_1 > 0.85$ . Two examples of these more synchronous trajectories are highlighted: the green trajectory in figure 11*a*, with  $t_1 = 0.05$ , and the blue trajectory in figure 11*c*, with  $t_1 = 0.11$ . The second group of trajectories form a dense band in the middle of the plots (near 0.14 in figure 11*a*), with much less variation in time. These trajectories are more metachronal, with  $0.15 < t_1 < 0.85$ . The yellow trajectory in figure 11*b* is an example of a more metachronal case, with  $t_1 = 0.17$ . As in the two-leg case, the more synchronous kinematics give more variation in body velocity.

In figure 11*d–f* we plot the average velocities exactly analogously to figure 8, and with the same parameters. Figure 11*f* gives the average velocities of the time traces in figure 11*a–c*. In each case there are four peaks at the  $t_1$  giving metachronal kinematics (0.2, 0.4, 0.6 and 0.8, shown by the arrows in figure 11*d*). The average velocity is only slightly lower between these  $t_1$ , in which case the kinematics are still close to metachronal. Only near  $t_1 = 0$  and 1 do we obtain a significant deviation from metachronal kinematics—synchronous

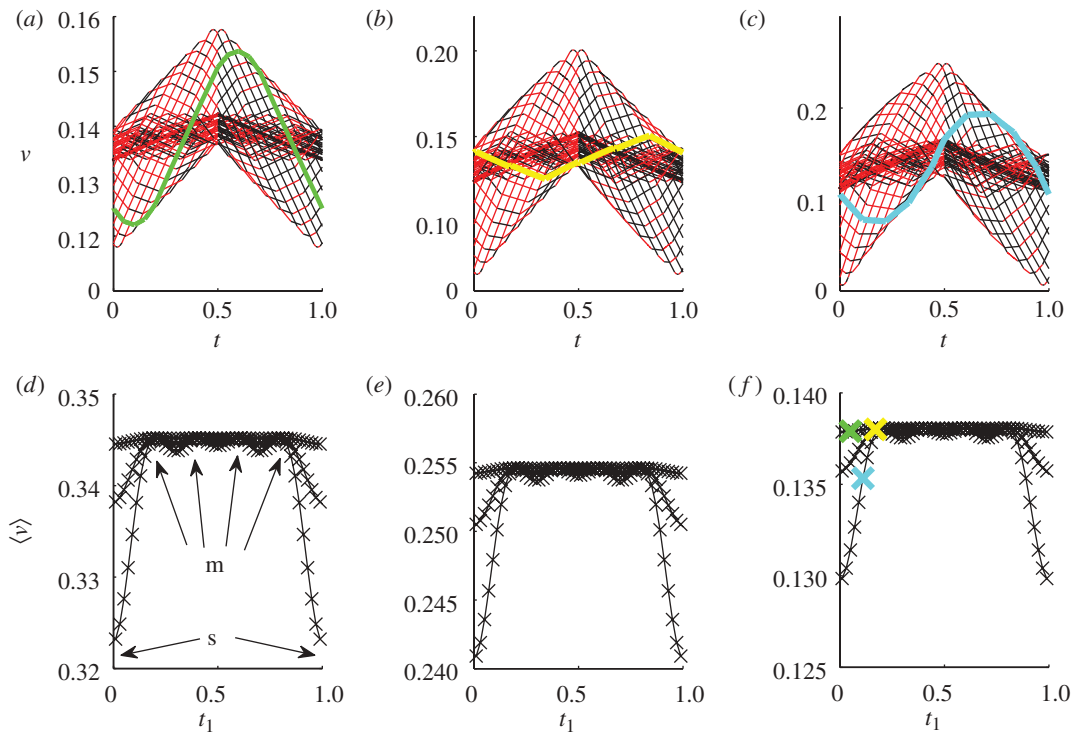


Figure 11. (a–c) For the quadratic drag law model with five legs, the body velocity over a period for the phase shift between the legs  $t_1$  varying from 0.01 to 0.99. In (a–c) the ratio of drag coefficients  $c_b : c_p : c_r$  is the same (1 : 0.08 : 0.04) but is multiplied by a constant factor of (a) 0.3, (b) 1 and (c) 1.9. (d–f) The average body velocity versus the phase difference between the legs,  $t_1$ , for three values of the ratio  $c_b : c_p : c_r$ , 1 : 0.28 : 0.04 (d), 1 : 0.16 : 0.04 (e) and 1 : 0.08 : 0.04 (f). In each panel, data are shown for three multiples of the given ratio: 0.3, 1 and 1.9. In each case curves with larger variations correspond to larger multiples. The data in (f) correspond to the plots in panels (a–c). As examples, the average velocities for single trajectories in panels (a–c) are shown in green (for  $t_1 = 0.05$ ), blue (for  $t_1 = 0.11$ ) and yellow (for  $t_1 = 0.17$ ). The arrows labelled ‘s’ and ‘m’ show the values of  $t_1$  that correspond to synchronous and metachronal kinematics, respectively.

kinematics (indicated by arrows)—and then the average velocities decrease significantly. The metachronal and synchronous velocities are nearly identical for five legs and for two legs (figure 8).

#### 4. SYNTHESIS

We have presented data from freely swimming and tethered krill which show that the swimming stroke is close to metachronal, with a nearly uniform phase shift between the five appendages. We have then applied a simple but general model to the free swimming of a body with drag-based propulsion. The model provides a quantitative basis for the intuition that metachronal kinematics are more effective than synchronous kinematics. In many cases this intuition was based on a quadratic scaling of drag with velocity. We have shown that metachronal kinematics lead to higher swimming speed for both linear and quadratic drag laws. We have also considered the kinematics in terms of mechanical efficiency—achieving the highest speed for a given input work. We have found that, for both the linear and quadratic drag laws, metachronal kinematics give the most efficient locomotion, although the speed advantage relative to synchronous kinematics is reduced when work is held fixed.

In future work we may consider organisms which use a combination of phases. For example, in copepods the

power stroke is metachronal, but the recovery stroke is synchronous (van Duren & Videler 2003; Catton *et al.* 2007). In the swimming of spiders on water surfaces, a variety of synchronous and metachronal motions have been observed (Suter *et al.* 2003). Furthermore, the recovery stroke for krill pleopods occurs with a somewhat higher velocity and shorter duration than the power stroke, as shown in figure 2. A future study may consider the effect of this stroke asymmetry. Another task for future experiments is to obtain body velocities for freely swimming krill and compare these with those of the model.

Analyses of juvenile stages of a large krill, *Euphausia superba* for example, of the same size but with a different number of pleopod pairs from the temperate species, *Euphausia pacifica*, may enable comparisons of the speed achieved with different numbers (2–5) of pleopod pairs. During ontogenetic development, pleopods are added to the posterior abdominal segments first, with each pair appearing initially as non-setose rudiments which become setose (i.e. hairy) at the next moult (Fraser 1936; Mauchline & Fisher 1969), thus increasing the pleopod’s profile area. An early larval stage can have two pairs of non-setose pleopods. The next stage has two pairs of setose and three pairs of non-setose pleopods and the final adult form has all five pairs of setose pleopods (see Knight 1984).

Here we have focused on the propulsor timing which maximizes the average body velocity. A synchronous

stroke cycle might be preferred in a short-time escape response. However, the initial advantage of the synchronous power stroke disappears once the propulsors need to perform the recovery stroke. Thus, for any swimming motion that lasts as long as a single stroke cycle or longer, we expect that metachronal kinematics are preferred.

We acknowledge support from NSF-DMS grant nos. 0810602 (S.A.) and 0531908 (S.A., K.S., J.Y.) and NSF-CBET grant 0625898 (J.Y.).

## APPENDIX A. DRAG COEFFICIENTS

We now relate the drag coefficients  $c_b$ ,  $c_p$ ,  $c_r$  we have defined to the most common drag coefficient at high Reynolds number, denoted  $C_D$ . For a body moving at speed  $V$  in a fluid at high Reynolds number,  $C_D$  is drag force divided by one-half the product of fluid density, velocity squared and profile area,  $C_D = 2D/\rho V^2 A_0$ . Our equations (3.1)–(3.4) are non-dimensionalized using the period of leg motion  $T$  as the characteristic time, the velocity  $V$  of the leg as the characteristic velocity, and the body mass plus added mass  $M$  as the characteristic mass. We now show how  $c_b$  is related to  $C_D$  for the body, which we denote  $C_{Db}$ ; analogous formulae relate  $c_p$  and  $c_r$  to  $C_{Dp}$  and  $C_{Dr}$ . In terms of  $C_{Db}$  and the other physical parameters, the first two terms in equation (3.1) are

$$\frac{MV}{T} \dot{v} = -\frac{1}{2} \rho V^\alpha A_{0b} C_{Db} \operatorname{sgn}(v) |v|^\alpha + \dots, \quad (\text{A } 1)$$

and, thus,

$$\dot{v} = -\frac{1}{2} \frac{\rho V^{\alpha-1} A_{0b} C_{Db} T}{M} \operatorname{sgn}(v) |v|^\alpha + \dots. \quad (\text{A } 2)$$

The last equation shows that  $c_b = \rho V^{\alpha-1} A_{0b} C_{Db} T/2M$ . Hence  $c_b$  is proportional to the term  $C_{Db}$ , which depends only on shape, and to  $A_{0b}$ , which is profile area. This fits with the intuition that drag force increases with size.

We may estimate the sizes of  $c_b$ ,  $c_p$  and  $c_r$  for a typical krill specimen using the following parameters:  $V = 20 \text{ cm s}^{-1}$ ,  $C_{Dp} = 2$ ,  $C_{Dr} = 2$  (drag coefficients for flat plates transverse to a flow),  $C_{Db} = 1$  (drag coefficient for a long cylinder with the long axis aligned with a flow; Batchelor 1967),  $T = 100 \text{ ms}$ ,  $A_{0b} = 100 \text{ mm}^2$ ,  $A_{0p} = 10 \text{ mm}^2$ ,  $A_{0r} = 5 \text{ mm}^2$ ,  $\alpha = 2$ ,  $M = \rho A_{0b} L$  with  $L = 3 \text{ cm}$ ,  $\rho = 1 \text{ g cm}^{-3}$ . We obtain  $c_b = 0.3$ ,  $c_p = 0.06$  and  $c_r = 0.03$ .

## REFERENCES

- Alben, S. 2008 An implicit method for coupled flow–body dynamics. *J. Comput. Phys.* **227**, 4912–4933. (doi:10.1016/j.jcp.2008.01.021)
- Alben, S. & Shelley, M. J. 2005 Coherent locomotion as an attracting state for a free flapping body. *Proc. Natl Acad. Sci. USA* **102**, 11 163–11 166. (doi:10.1073/pnas.0505064102)
- Alexander, D. E. 1988 Kinematics of swimming in two species of *Idotea* (Isopoda: Valvifera). *J. Exp. Biol.* **138**, 37.
- Andersen, A., Pesavento, U. & Wang, Z. J. 2005 Analysis of transitions between fluttering, tumbling and steady descent of falling cards. *J. Fluid Mech.* **541**, 91–104. (doi:10.1017/S0022112005005847)
- Batchelor, G. K. 1967 *An introduction to fluid mechanics*. Cambridge, UK: Cambridge University Press.
- Baudouin, A. & Hawkins, D. 2004 Investigation of biomechanical factors affecting rowing performance. *J. Biomech.* **37**, 969–976. (doi:10.1016/j.jbiomech.2003.11.011)
- Billings, B. H., Gray, D. E., Bleil, D. F. & Bennett, A. A. 1963 *American institute of physics handbook*. London, UK: McGraw-Hill.
- Blake, R. W. 1981 Mechanics of drag-based mechanisms of propulsion in aquatic vertebrates. *Symp. Zool. Soc. Lond.* **48**, 29–52.
- Blake, R. W. 1983 *Fish locomotion*. Cambridge, UK: Cambridge University Press.
- Brown, P. P. & Lawler, D. F. 2003 Sphere drag and settling velocity revisited. *J. Environ. Eng.* **129**, 222–231. (doi:10.1061/(ASCE)0733-9372(2003)129:3(222))
- Cabrera, D., Ruina, A. & Kleshnev, V. 2006 A simple 1+ dimensional model of rowing mimics observed forces and motions. *Hum. Move. Sci.* **25**, 192–220. (doi:10.1016/j.humov.2005.11.002)
- Catton, K. B., Webster, D. R., Brown, J. & Yen, J. 2007 Quantitative analysis of tethered and free-swimming copepodid flow fields. *J. Exp. Biol.* **210**, 299–310. (doi:10.1242/jeb.02633)
- Childress, S. 1981 *Mechanics of swimming and flying*. Cambridge, UK: Cambridge University Press.
- Cohen, E. E. A., Ejsmond-Frey, R., Knight, N. & Dunbar, R. I. M. 2010 Rowers' high: behavioural synchrony is correlated with elevated pain thresholds. *Biol. Lett.* **6**, 106–108. (doi:10.1098/rsbl.2009.0670)
- Fraser, F. C. 1936 *On the development and distribution of the young stages of krill (Euphausia superba)*. Cambridge, UK: Cambridge University Press.
- Hamner, W. M. 1990 Design developments in the planktonkreisel, a plankton aquarium for ships at sea. *J. Plank. Res.* **12**, 397–402. (doi:10.1093/plankt/12.2.397)
- Hill, H. & Fahrig, S. 2009 The impact of fluctuations in boat velocity during the rowing cycle on race time. *Scand. J. Med. Sci. Sports* **19**, 585–594. (doi:10.1111/j.1600-0838.2008.00819.x)
- Kils, U. 1981 *The swimming behavior, swimming performance and energy balance of Antarctic krill, Euphausia superba*. Cambridge, UK: SCAR and SCOR, Scott Polar Research Institute.
- Knight, M. D. 1984 Variation in larval morphogenesis within the southern California bight population of *Euphausia pacifica* from winter through summer, 1977–1978. *California Cooperative Oceanic Fisheries Investigations Atlas* **87**, 87–99.
- Mauchline, J. & Fisher, L. R. 1969 The biology of euphausiids. *Adv. Mar. Biol.* **7**, 1–454.
- Morgan, E. 1972 The swimming of Nymphon gracile (Pycnogonida): the swimming gait. *J. Exp. Biol.* **56**, 421–432.
- Neumeister, J. 2004 Rhythm on the river. *New Sci.* **30**.
- Nicol, S. & Endo, Y. 1997 *Krill fisheries of the world*. Technical paper no. 367. Rome, Italy: Food and Agriculture Organization.
- Nolte, V. 2007 Out of sync, out of mind? *Rowing News* **14**, 62–65.
- Rensen, J., Bosman, D., Magnaudet, J., Ohl, C. D., Prosperetti, A., Togel, R., Versluis, M. & Lohse, D. 2001 Spiraling bubbles: how acoustic and hydrodynamic forces compete. *Phys. Rev. Lett.* **86**, 4819–4822. (doi:10.1103/PhysRevLett.86.4819)

- Suter, R. B., Stratton, G. & Miller, P. R. 2003 Water surface locomotion by spiders: distinct gaits in diverse families. *J. Arachnol.* **31**, 428–432. (doi:10.1636/m02-22)
- Swadlow, K. M., Ritz, D. A., Nicol, S., Osborn, J. E. & Gurney, L. J. 2005 Respiration rate and cost of swimming for Antarctic krill, *Euphausia superba*, in large groups in the laboratory. *Mar. Biol.* **146**, 1169–1175. (doi:10.1007/s00227-004-1519-z)
- Thompson, B. G. & Smith, P. A. 2004 An experiment in rotational motion with linear and quadratic drag. *Am. J. Phys.* **72**, 839. (doi:10.1119/1.1632493)
- van Duren, L. A. & Videler, J. J. 2003 Escape from viscosity: the kinematics and hydrodynamics of copepod foraging and escape swimming. *J. Exp. Biol.* **206**, 269–279. (doi:10.1242/jeb.00079)
- Vogel, S. 1994 *Life in moving fluids: the physical biology of flow*. Princeton, NJ: Princeton University Press.
- Walker, J. A. & Westneat, M. W. 2000 Mechanical performance of aquatic rowing and flying. *Proc. R. Soc. Lond. B* **267**, 1875–1881. (doi:10.1098/rspb.2000.1224)
- Wing, A. M. & Woodburn, C. 1995 The coordination and consistency of rowers in a racing eight. *J. Sports Sci.* **13**, 187–197. (doi:10.1080/02640419508732227)
- Yen, J., Brown, J. & Webster, D. R. 2003 Analysis of the flow field of the krill, *Euphausia pacifica*. *Mar. Freshwater Behav. Physiol.* **36**, 307–319. (doi:10.1080/10236240310001614439)